

**Titre:** Three-dimensional printing of freeform helical microstructures: a review  
Title:

**Auteurs:** Rouhollah Dermanaki Farahani, Kambiz Chizari, & Daniel Therriault  
Authors:

**Date:** 2014

**Type:** Article de revue / Article

**Référence:** Farahani, R. D., Chizari, K., & Therriault, D. (2014). Three-dimensional printing of freeform helical microstructures: a review. *Nanoscale*, 6(18), 10470-10485.  
Citation: <https://doi.org/10.1039/c4nr02041c>

## Document en libre accès dans PolyPublie

**URL de PolyPublie:** <https://publications.polymtl.ca/10407/>  
PolyPublie URL:

**Version:** Version finale avant publication / Accepted version  
Révisé par les pairs / Refereed

**Conditions d'utilisation:** Tous droits réservés / All rights reserved  
Terms of Use:

## Document publié chez l'éditeur officiel

**Titre de la revue:** *Nanoscale* (vol. 6, no. 18)  
Journal Title:

**Maison d'édition:** Royal Society of Chemistry  
Publisher:

**URL officiel:** <https://doi.org/10.1039/c4nr02041c>  
Official URL:

**Mention légale:** © 2014. This is the author's version of an article that appeared in *Nanoscale* (vol. 6, no. 18) . The final published version is available at <https://doi.org/10.1039/c4nr02041c>  
Legal notice:

## ARTICLE

# Three-Dimensional Printing of Freeform Helical Microstructures: A Review

Cite this: DOI: 10.1039/x0xx00000x

R.D. Farahani, K. Chizari and D. Therriault\*

Received 00th January 2012,  
Accepted 00th January 2012

DOI: 10.1039/x0xx00000x

www.rsc.org/

Three-dimensional (3D) printing is a fabrication method that enables creation of structures from digital models. Among the different structures fabricated by 3D printing methods, helical microstructures attracted the attention of the researchers due to their potential in different fields such as MEMS, lab on a chip systems, microelectronics and telecommunications. Here we review different types of 3D printing methods capable of fabricating 3D freeform helical microstructures. The techniques including two more common microfabrication methods (i.e., Focused ion beam chemical vapour deposition and microsteolithography) and also five methods based on computer-controlled robotic direct deposition of ink filament (i.e., fused deposition modeling, meniscus-confined electrodeposition, conformal printing on a rotating mandrel, UV-assisted and solvent-cast 3D printings) and their advantages and disadvantages regarding their utilization for the fabrication of helical microstructures are discussed. Focused ion beam chemical vapour deposition and microsteolithography techniques enable the fabrication of very precise shapes with a resolution down to ~100 nm. However, these techniques may have material constraints (e.g., low viscosity) and/or may need special process conditions (e.g., vacuum chamber) and expensive equipment. The five other techniques based on robotic extrusion of materials through a nozzle are relatively cost-effective, however show lower resolution and less precise features. The popular fused deposition modeling method offers a wide variety of printable materials but the helical microstructures manufactured featured a less precise geometry compared to the other printing methods discussed in this review. The UV-assisted and the solvent-cast 3D printing methods both demonstrated high performance for the printing of 3D freeform structures such as the helix shape. However, the compatible materials used in these methods were limited to UV-curable polymers and Polylactic acid (PLA), respectively. Meniscus-confined electrodeposition is a flexible, low cost technique that is capable of fabricating 3D structures both in nano- and microscales including freeform helical microstructures (down to few microns) at room conditions using metals. However, the metals suitable for this technique are limited to those can be electrochemically deposited with the use of an electrolyte solution. The highest precision on the helix geometry was achieved using the conformal printing on a rotating mandrel. This method offers the lowest shape deformation after printing but requires more tools (e.g., mandrel, motor) and the printed structure must be separated from the mandrel. Helical microstructures made of multifunctional materials (e.g., carbon nanotube nanocomposites, metallic coated polymer template) were used in different technological applications such as strain/load sensors, cell separators and micro-antennas. These innovative 3D microsystems exploiting the unique helix shape demonstrated their potential for better performance and more compact microsystems.

## 1 Introduction

2 Three-dimensional (3D) printing is a flexible manufacturing  
3 method that enables fabrication of objects based on a computer  
4 designed models with complex 3D features for a wide variety  
5 applications.<sup>1, 2</sup> The diversity of the materials used in 3D printing  
6 methods is constantly increasing enabling the printing of  
7 structures made of polymers, ceramics and metals.<sup>2</sup> Various

8 structures in different sizes, from size of a house to submicron,  
9 can be made using different types of 3D printing methods.<sup>3, 4</sup>  
10 These techniques enable building 3D miniaturized microsystems  
11 with smaller planar footprint while keeping its high performance  
12 compared to two-dimensional (2D) structures. Various complex  
13 3D features including supported<sup>1, 5</sup> (i.e., layer-by-layer) and self-  
14 supported<sup>5</sup> (e.g., spanning filament<sup>6</sup>) structures can be fabricated

using most of the 3D printing techniques. However, construction of 3D freeform microstructures like helical geometries without the need to be supported by the underlying layers still remains a challenging problem.<sup>7-9</sup> The fabrication of such structures is also difficult and costly using conventional lithography techniques. 3D helical microstructures with feature sizes of a few hundred microns exhibit high potential for a broad range of applications in microsystems. The geometry of the helical microstructures usually of importance to deliver desired properties for a target application. The helical geometry might be the overall size of the structure, numbers of turns in a coil, pitch, diameter of the coil and diameter of the filament. For instance, the performance of a helical microstructure antenna can be optimized by controlling its geometry for narrowband and broadband design.<sup>10</sup> Depending on the properties of the materials (e.g., mechanical, electrical, thermal and chemical properties), the 3D helical microstructures have high potential to replace 2D components for different applications such as micro electromechanical systems (MEMS),<sup>11-13</sup> electrodes for lab-on-a-chip systems,<sup>14-16</sup> microelectronics<sup>17-20</sup> and several other systems. Several microfabrication techniques have emerged to fabricate 3D freeform microstructures such as photolithography techniques,<sup>12, 13</sup> chemical laser vapor deposition,<sup>18</sup> fused deposition modelling,<sup>21</sup> two-photon polymerization<sup>22, 23</sup> and direct-write techniques.<sup>24, 25</sup> Table 1 lists various selected microfabrication techniques compatible for 3D freeform fabrication as well as materials used for each technique. In addition, it is shown in the table if the techniques have been used for the fabrication of 3D helical microstructures. The goal of this paper is to review several 3D printing techniques suitable for the fabrication of helical freeform microstructures (shown in bold in Table 1). Other techniques such as liquid rope coiling of viscous fluids<sup>26</sup> have been also used for the fabrication of helical microstructures. In the rope coiling method using a spinning process, cellulose-based solution was extruded at the surface of a mobile coagulation bath that led to the fabrication of helical microcoils as a result of buckling instability. The fabrication of very long coils (up to the length of the coagulating bath) with diameters ranging 100-400  $\mu\text{m}$  and the filament diameter of 300-700  $\mu\text{m}$  has been reported. However, such techniques are not discussed in this review paper since it focuses on the 3D printing methods. Therefore, the paper is organized as follows: two more common methods (i.e., focused ion beam chemical vapor deposition and microstereolithography) including their capabilities and limitations are first discussed. Then, the 3D printing techniques based on direct ink deposition for helical microstructures and the limitations/difficulties to fabricate helical microstructures are then presented. This is followed by the introduction of the five 3D printing methods (i.e. fused deposition modeling, meniscus-confined electrodeposition, conformal printing on a rotating mandrel, UV-assisted and solvent-cast 3D printings), providing detailed information for each technique and materials used for the fabrication of helical microstructures. The applications of helical microstructures in different fields such as MEMS, lab on a chip systems, microelectronics and telecommunications are discussed in details. One of the main outcomes of this review is to guide the reader to find the most suitable 3D printing technique for the fabrication of helical microstructure with the desired geometry for the targeted application.

## 3D printing of helical microstructures based on two popular microfabrication techniques

### 1. Focused ion beam chemical vapor deposition (FIB-CVD)

FIB-CVD is an additive manufacturing technique which is widely used for the deposition of materials in an arbitrary shape with a size ranging from nanometers to hundreds of micrometers.<sup>27, 28</sup> Figure 1 schematically represents the FIB-CVD method based on localized chemical vapor deposition using FIB. The FIB-CVD consists of a nozzle that injects the reactive gaseous material into a vacuum chamber at a desired position close to a substrate usually a silicon substrate, followed by a chemical reaction caused by a focused ion beam that solidifies the gas materials (i.e., materials deposition). As opposed to the other techniques presented in this review paper that use liquid or melted polymers as constructing materials, the FIB-CVD technique uses gases such as tungsten hexacarbonyl and phenanthrene which are reactive organic gases.<sup>27</sup> The precursor gas from a heated container is injected into a vacuum chamber by a fine micronozzle located above the substrate at desired angle. The FIB is then scanned in the desired location using a computer-controlled system in order to build the programmed patterns. The material deposition occurs as a result of reaction between FIB and precursor gas where the FIB meets the gas. The reaction results in decomposition of the precursor into volatile and non-volatile components. The latter remains on the reaction region as deposited material to create the shape of interest. The thickness of the deposited materials depends on the irradiation time which is controlled by the scanning speed.<sup>27, 29</sup>

In addition to helical microstructures, the FIB-CVD technique enables the fabrication of other shapes with supported and freeform geometries. Compared to the other techniques, the FIB-CVD can fabricate very precise shapes with a resolution down to  $\sim 100$  nm.<sup>27</sup> The high resolution and precision comes from the fact that the materials used in this method are in gas state which is easy to inject through fine nozzles. The beam diameter can be as small as several nanometers with a short penetration depth of a few tens of nanometers. Matsui *et al.*<sup>27</sup> used this technique to fabricate various structures with different shapes for MEMS and NEMS applications. Depending on the shape and size of the fabricated structures, they reported a beam current of 0.4 pA to 120 pA and a fabrication time of 40 s to 2.5 h. Figure 1b shows a SEM image of the fabricated helical structure, composed of three turns with a coil diameter of 0.6  $\mu\text{m}$ , a coil pitch of 0.7  $\mu\text{m}$  and a filament diameter of 0.08  $\mu\text{m}$ . The irradiation time was 40 s at a beam current of 0.4 pA. They used two commercially available FIB systems (SMI9200, SMI2050, SII Nanotechnology Inc., Tokyo, Japan) with a  $\text{Ga}^+$  ion beam and a phenanthrene as precursor gas and nozzle's internal diameter of 0.3 mm. However, the main drawback of this method is its high cost of equipment which is about \$800,000. Moreover, the technique limited by material constraints and works only in a high vacuum environment.

### 2. Microstereolithography (MSL)

Stereolithography (SL) is a popular conventional method for the fabrication of 2D and 3D microstructures using photopolymers.<sup>12, 30</sup> In this technique, a focused ultraviolet (UV) laser beam scans a liquid photopolymer inside a container and selectively cures the photopolymer in the desired locations or paths to form the first layer of the desired solid structure. The UV system is mounted onto a movable platform which moves vertically deeper into the liquid. This allows to successively create other layers on the top of each other, resulting in a 3D part. Microstereolithography (MSL) works with the

same principle as SL, but with a pattern resolution of several microns.<sup>30</sup> Figure 2(a) shows schematics of the fabrication process. New techniques based on MSL such as scanning-based technique and two-photon polymerization<sup>22</sup> have emerged to improve the resolution of the MSL technique by controlling penetration of light into the photopolymer resin. Those techniques have been developed with the aim at reducing cure depth in MSL which results in more precise features. The main drawback of MSL is the material limitations since the technique can only work with low viscosity materials. In addition, the equipment usually cost between \$200,000 – \$600,000. Choi et al.<sup>30</sup> reported the use of light absorber blended with the photopolymer to control the depth of cure using a dynamic mask projection MSL (Figure 2). Upon controlling the depth of cure, they have been able to fabricate freeform helical microstructures. Figure 2b and 2c show an individual microcoil and a network consisting of four identical microcoils with the coil's diameter of 500  $\mu\text{m}$  and the filament's diameter of 130  $\mu\text{m}$ . The fabrication conditions were a layer thickness of 4  $\mu\text{m}$  with a total layer number of 298 with exposure energy of 33.8  $\text{mJ}/\text{cm}^2$ , which was corresponded to an exposure time of 1 s. The material used for the fabrication of the helical microcoil was an acrylate-based commercial resin blend (HDDA, Miwon Commercial Co., and BEDA, Hannong Chemicals Inc.) mixed with 1 wt.% of a photoinitiator (DMPA, Fisher Scientific Inc.) and 0.15 wt.% Tinuvin 327<sup>TM</sup> (Ciba, Timonium) as the photoabsorber. The accuracy for the fabrication of 3D helical microcoils in this technique depends on the exposure energy/time and the materials used, specifically the concentration of the photoabsorber. They showed that the light penetration depth and thus, the cure depth reduced by the increase of photoabsorber concentrations, resulting in higher accuracy for the fabrication of the helical microcoils.

### 3D printing of helical microstructures based on robotic direct deposition of ink filament

Direct-write techniques mainly consist of the deposition of continuous ink filaments that allowed the construction of 3D devices through a layer-by-layer building sequence.<sup>31, 32</sup> Figure 3 shows a typical direct-writing setup, which is composed of a computer-controlled robot that moves a dispensing apparatus along the  $x$ ,  $y$  and  $z$ , axes. Figure 3b shows schematically the deposition of the ink materials on a substrate that leads to a helical pattern, as the first layer of a 3D scaffold structure. The following layers are then deposited by incrementing the  $z$ -position of the extrusion nozzle, resulting in a periodic microstructure featuring several layers (Figure 3c). The material's viscosity is one of the most important properties for an accurate fabrication using these techniques.<sup>31, 33</sup> The viscosity should be low to moderate to enable the material extrusion through fine micro-nozzles for the maximum extrusion pressure achievable. On the other hand, the increase of material rigidity right after extrusion is a must for filament shape retention.<sup>31</sup> Various materials and techniques have been used to achieve the filament's rigidity required for the direct-write fabrication of microstructures. Organic fugitive inks possessing a shear thinning rheological behavior (i.e., a decrease of viscosity with an increase of shear forces inside the nozzle) are found to be ideal materials.<sup>31</sup> These inks have been used for the layer-by-layer fabrication of periodic micro-scaffolds.<sup>31, 32, 34-36</sup> However,

to fabricate freeform 3D structures such as helical microstructures, a further increase of rigidity is required. In this review paper, five different 3D printing techniques, based on direct deposition of ink materials which have been demonstrated for the fabrication of helical microstructures are presented: fused deposition modeling (FDM), meniscus-confined electrodeposition (MCED), UV-assisted 3D printing (UV-3DP), solvent-cast 3D printing (SC-3DP), and conformal printing on rotating mandrel (CPRM). In these techniques, the increase of rigidity required for the fabrication of helical microstructures is achieved through different mechanisms which will be thoroughly discussed in the following sections. A summary table comparing advantages, limitations and potential applications of the five techniques will be later provided in this review paper as Table 3. These five techniques are based on the same principle of the direct deposition of filaments using a computer-controlled extruding robot. FDM is a well-known fabrication technique which has been vastly used in the literature. MCED is a very precise method that uses the thermodynamic stability of a liquid meniscus. The material deposition path in 3D space is controlled by piezostages in order to directly print 3D microstructures. The other three 3D printing techniques, which have been recently developed, are customized versions of the method shown in Figure 3. The robot used for these three techniques is a commercially available robot (I & J2200-4, I & J Finsar) consisting of a moving stage along the  $x$ -axis and a robot head moving in the  $y$ - $z$  plane that is computer controlled with commercial software (JR Point dispensing). The dispensing apparatus (HP-7X, EFD) mounted on the robot head carries the ink material, which is extruded by an applied pressure using a pneumatic fluid dispenser (Ultra<sup>TM</sup> 2400 series, EFD). In order to print the helical structure the ink material should be extruded in a circular form on the substrate while the extrusion nozzle moves upwards in the  $z$  direction keeping its circular movement in  $x$ - $y$  direction. The diameter of the helical structure and the pitch can be varied by giving the desired coordination to the dispensing robot which provides the possibility of fabrication of a helical structure with various pitches and diameters. Although microstructures with other geometries are not the concern of this review paper, the four techniques discussed here are capable of fabricating other complex geometries such as microstructure for potential tissue engineering,<sup>37</sup> vertical microrod network<sup>38</sup> for potential lab-on-a-chip and square towers for MEMS applications.<sup>37</sup>

#### 1. Fused deposition modeling (FDM)

In this method, the ink is heated until it melts or softens and then is extruded from a nozzle on a substrate to build a structure in a layer-by-layer manner. The extruded ink solidifies when its temperature lowers due to air convection post-extrusion. Figure 4 schematically represents the FDM method<sup>39</sup> which is widely used in commercial 3D printers for different materials such as polymers, metals and ceramic filled polymers.<sup>40-42</sup> The most frequently used polymers are thermoplastics such as acrylonitrile butadiene styrene (ABS) and PLA.<sup>43-46</sup> The cost of the 3D printers varies from about \$200 to about \$330,000 depending on the manufacturing company, resolution of the printer and size of the printable object.<sup>47</sup> In this method the ink, usually in the form of spooled filament, is fed into a heated chamber connected to an extrusion nozzle. The advantage of this method compared to the other 3D printing methods discussed in this review is the possibility of the utilization of a relatively wide variety of ink materials. One of the most important properties required for the FDM ink is to melt or soften at high temperatures in order to be able to be extruded through the nozzle. The main drawback of

this method is that it is a high temperature 3D printing method which can cause some difficulties for freeform features and limitations concerning the materials that degrades at high temperatures. Since the glass transition temperature of polymers alters from one to another, the temperature of the heating chamber and the temperature tolerance of the extrusion components should be well adjusted for accurate printing. Yamada *et al.* used FDM to print 3D structures at the microscale.<sup>21</sup> Various nozzles (internal diameter range: 0.05–0.25 mm), extrusion rates (0.01–100 mm<sup>3</sup>/min), stage scanning speeds (5–200 mm/min, materials (PLA, Poly(glycolic acid) (PGA) and polylactic-co-glycolic acid (PLGA)) and heating chamber temperatures (170–235 °C) were used in this work for 3D printing of different microstructures. The optimal nozzle diameter depends on the size and design accuracy of the structure needed to be fabricated. The nozzles with fine ID size such as 50 µm enable fabrication of microstructures with high resolutions. The temperature of the heating chamber depends on the melting temperature of the polymer used as the ink. The extrusion rate plays an important role on the precision of the printed patterns as the high extrusion speed leads to the formation of lumps and in contrast low extrusion speed leads to a broken or non-continuous printed patterns. They showed the possibility of freeform 3D printing of helical structures by FDM using PLGA as the ink material. Figure 4c shows an optical image of the fabricated helical microstructure, composed of 20 turns with a pitch of ~0.8 mm. The coil's diameter is ~0.9 mm and the filament's diameter is ~200 µm. This diameter can be reduced to about 45 µm in self-stand 3D printing in the form of micro-pipe. In another work, Safari *et al.* used this method to make a helical electrode using an alloy of silver-palladium on a piezoelectric tube.<sup>40</sup> In this work, a piezoelectric tube was placed on a rotating shaft and the electrode was deposited on the surface of the tube while the nozzle moved forward, resulting in a helical shaped electrode with a diameter of 1.78 mm.

Despite the vast application of FDM method in 3D printing, very few publications were involving the freeform printing of helical microstructures. This can be explained by the difficulty of fabrication of helical microstructures with the predetermined diameter and pitch as the printed structure can be deformed during the cooling and hardening of the extruded material.

## 2. Meniscus-confined electrodeposition (MCED)

MCED is an electrodeposition method that uses the thermodynamic stability of a liquid meniscus to directly print 3D microstructures. The MCED is capable of fabricating 3D structures of designed shapes and sizes in nano- and microscales including freeform helical microstructures (down to few microns) at room conditions using metals such as copper and platinum.<sup>49</sup> Figure 5 schematically represents this technique which consists of long-travel piezoelectric movement of a micropipette containing an electrolyte solution along the desired 3D trajectory. Dispensing micronozzles with internal diameters ranging from 100 nm to tens of microns can be mounted onto the micropipette in order to control the feature size of the structures. The micropipette is moved toward the conductive substrate and an electrical potential is applied between the electrolyte and the substrate. At the appropriate distance, the meniscus is formed between the substrate and the micronozzle and thereby the electrodeposition is initiated onto the substrate. The dispensing micronozzle is then moved away from the substrate at a calibrated speed that matched the deposition speed in order to keep meniscus formation between the nozzle and the deposited materials, allowing continuous fabrication. Hu *et al.* reported the use of this technique to fabricate 3D freeform

micro- and nanostructures. Figure 5b shows a SEM image of an array of Cu helical microcoils. The coils were solid, nanocrystalline and highly conductive as bulk metal.<sup>48, 49</sup>

The feature size using the MCED technique is influenced by several parameters such as the nozzle's diameter, its moving speed, the thermodynamic properties of the electrolyte solution, and the electrodeposition and substrate surface interaction. Several metals such as Cu, Pt, Co, Ni, Au have been successfully used in this technique to fabricate micro- and nanostructures. The main advantages of the technique are its flexibility to fabricate nanoscale structures and also its relatively low cost compared to traditional lithography techniques. However, the materials suitable for this technique are limited to metals and specifically those that can be electrochemically deposited with the use of an electrolyte solution.<sup>48</sup>

## 3. UV-assisted 3D printing (UV-3DP)

The UV-3DP technique relies on the robotically-controlled micro-extrusion of a UV-curable ink filament while the extrusion point is moved in three directions. The resolution of the robot in x and y axes is 5 µm and in z axis is 2.5 µm. The uncured material is photopolymerized within seconds after extrusion under UV exposure. Figure 6a and 6b represents a schematic of the UV-3DP fabrication of a freeform helical microstructure. The UV light-emission setup is installed on the robot head and follows the extrusion point. A set of six optical fibers arranged in a circular pattern (Figure 6b) delivers the UV light which is provided by two high-intensity UV light-emitting diodes (LED, NCSU033A, Nichia) having a wavelength centered at 365 nm close to the extrusion point at the tip of the extrusion micronozzle (Precision Stainless Steel Tips, EFD). The intensity of the present UV radiation is 50 mWcm<sup>-2</sup> which can be increased by using UV light-emitting diodes with higher intensities and also adding extra LEDs.

The ink material must meet a few criteria to be suitable for the UV-3DP. First, a very high polymerization rate of the ink is essential for phase changes from liquid to solid within seconds under the UV illumination. Numerous UV-curable materials are commercially available which allow the design or selection of a desired ink, depending on the curing rate and product properties. For instance, acrylate-based resins which are the most commonly used UV-curable materials exhibit a fast reactivity.<sup>50</sup> Second, materials with moderate to high viscosities are necessary to extrude stable filaments. Low viscosity leads to excessive sagging of the extruded materials prior to curing under the UV illumination.<sup>38</sup> Table 2 lists the materials used for the fabrication of 3D helical microstructures using the UV-3DP technique. The viscosity increase achieved by adding nanofillers (e.g., carbon nanotubes and silica nanoparticles) to the pure resins with low viscosity enabled a successful UV-3D printing. One of the most important advantages of the UV-3DP technique over the conventional microfabrication techniques (e.g., two-photon polymerization) is its capability of fabricating microdevices from non-transparent nanocomposites. However, the addition of higher loadings, especially in case of carbon nanotubes (above 2 wt.%) may decrease the materials transparency and consequently their photopolymerization rates. In addition, the increase of viscosity may cause problems for the materials extrusion through fine nozzles (e.g., internal diameter (ID) below 100 µm) and, thus affect minimum filament diameter achievable.

In addition to the materials criteria mentioned above, processing parameters have also to be carefully tailored. For successful and accurate freeform fabrication of 3D helical structures, the extrusion speed, the pressure applied to the material, and the UV-

radiation intensity have to be adjusted according to the viscosity and the curing rate of the materials. The extruded filament must stay under the UV-exposure for a certain time until it reaches sufficient rigidity for self-support. Increasing the exposure time and the intensity of the UV-radiation lead to a higher solidification rate of the material. However, the detailed effect of the exposure time on the geometry of helical structures is very complicated, as it is not an independent parameter and depends on: the UV-exposure zone, the designed extrusion path and the deposition speed. The intensity of the current UV setup is limited to a constant value ( $50 \text{ mW}\cdot\text{cm}^{-2}$ ). Further publication would be foreseen to study those effects on the geometry of the helical microstructures (e.g., by increasing the intensity using high power UV setup). Figure 6c shows SEM images of a helical microstructure composed of 5 turns with a pitch of  $\sim 1 \text{ mm}$ . The coil's diameter is  $\sim 1 \text{ mm}$  and the filament's diameter is about  $200 \mu\text{m}$ . The microcoil was fabricated with the urethane-based resin (NEA123T) using a micronozzle with the ID of  $150 \mu\text{m}$  at an extrusion speed of  $0.3 \text{ mm/s}$  and an extrusion pressure of  $2 \text{ MPa}$ . The fabricated structure geometry closely matched the programmed path due to the appropriate selection of processing parameter values.

The influence of several parameters such as extrusion speed, extrusion pressure and viscosity of materials has been studied in the fabrication of 3D microstructures including 3D freeform helical microcoils using the UV-3D printing of UV-curable thermosetting resins and their associated nanocomposite materials.<sup>38</sup> A processing map has been defined in order to help choosing the proper parameters for the UV-3D printing of microstructures with various geometries. That map may offer a general overview of the technique with its capabilities and can be used as a guide for the fabrication of different 3D geometries including helical microcoils. It has been shown that the processing zone is much narrower for the fabrication of helical freeform structures when compared to layer-by-layer supported microscallops. For freeform structures, high solidification rate is required, which limits the range of applicable extrusion pressures and speeds. In this case, a slight mismatch between the processing parameters affects the fabricated structure shapes which may be far from the programmed trajectory. However, the fabrication of 3D helical microcoils was successful with few nozzles (internal diameter range:  $100\text{--}200 \mu\text{m}$ ), deposition speed of  $0.2\text{--}0.5 \text{ mm/s}$  and extrusion pressure of  $0.5\text{--}2.5 \text{ MPa}$ , and material's viscosity of  $70\text{--}250 \text{ Pa}\cdot\text{s}$  (at low shear rates).

#### 4. Solvent-cast 3D printing (SC-3DP)

The SC-3DP method is based on the extrusion of a polymer dissolved in a volatile solvent, under an applied pressure. Figure 7 shows a schematic of the fabrication process using the SC-3DP method. The dissolution of the polymer in the solvent lowers its viscosity and facilitates its extrusion. The evaporation of solvent increases the rigidity of the ink and changes its fluid-like form into solid-like which enables the shape retention of the deposited material. The required equipment for this method is mainly a micropositioning robot, a controlled pressure dispenser and a syringe filled with the polymer solution connected to a micronozzle. In order to be able to print 3D freeform structures which retain their form after printing, the selected solvent, polymer and their relative concentration should be set so that the ink solution can easily exit from the micronozzle but quickly dries as it exits the micronozzle. Different processing parameters such as the extrusion speed and the extrusion pressure can affect the shape retention of the structure. Guo *et al.* reported

use of polylactic acid (PLA) solution in dichloromethane (DCM) for 3D freeform printing of a helical microstructure.<sup>24</sup> Figure 7c shows SEM images of a helical microstructure composed of eight  $1 \text{ mm}$  diameter turns, a pitch of  $0.7 \text{ mm}$  and the filament's diameter of  $\sim 200 \mu\text{m}$ . The fabrication was carried out with  $30 \text{ wt.}\%$  PLA solution using a micronozzle with the ID of  $100 \mu\text{m}$  at an extrusion speed of  $0.1 \text{ mm/s}$  and an extrusion pressure of  $1.75 \text{ MPa}$ . DCM was chosen due to its fast evaporation as its boiling point is very low ( $39.6^\circ\text{C}$ ) compared to other solvents that dissolve PLA. Based on their results the best concentration of PLA in DCM is about  $30 \text{ wt.}\%$  in order to have enough viscosity so it can keep its shape after extrusion. Higher concentrations of PLA increased the viscosity of the inks which would cause some difficulties for their extrusion while low concentrations of PLA would lead to a significant structural deformation after the extrusion. The ID of the nozzle can also influence the 3D freeform structure retention. The structures printed with smaller nozzle's ID (i.e.,  $100 \mu\text{m}$ ) have better retention compared to the ones printed with bigger nozzle's IDs since DCM evaporates faster, due to its lower diffusion distance, when the diameter of the printed filament is smaller.

The materials used for solvent-cast printing are limited to the polymers that can be dissolved in solvents with low boiling points because the retention of the object printed by this method depends on the speed of solvent evaporation. To the best of our knowledge the only used polymer/solvent for freeform solvent-cast 3D printing so far was PLA/DCM. Polymers and solvents that have been used for melt spinning and electro-spinning methods are potential candidates for other inks since those methods are also involving the fast evaporation of solvent from polymer fibers. More than 40 polymers and the corresponding solvents are listed in a review article written by Huang *et al.*<sup>51</sup> Some of the outstanding advantages of this method is its simplicity and the possibility of printing at room temperature. The resolution of the printing pattern depends on the resolution of the dispensing robot ( $x$  &  $y$  axes:  $5 \mu\text{m}$  and  $z$  axis:  $2.5 \mu\text{m}$ ) and the diameter of the printing filament depends on the internal diameter of the extrusion micronozzle. The minimum diameter of the extruded filament reported for freeform SC-3DP method is  $\sim 100 \mu\text{m}$ .<sup>24</sup> In this project, the cost of the dispensing robot together with the air-operated dispenser was  $\sim \$12,000$ .

#### 5. Conformal printing on rotating mandrel (CPRM)

This method consists of a dispensing system that extrudes the ink directly onto a cylindrical rotating mandrel. As the extrusion continues, the mandrel or the extrusion nozzle moves along the direction of the rotating mandrel and the extruded ink creates a helical form around the mandrel. This method requires an extruding robot together with a controllable rotation speed mandrel (Figure 8). The mandrel can be rotated and moved along the  $x$  axis with a resolution of  $0.4 \mu\text{m}$  by using MICOS stepper motors. The cost of the stepper motors together with the dispensing apparatus is  $\sim \$4,000$ . The diameter of the helical structure and the helix pitch depend on the diameter of the rotating mandrel and the displacement speed of the extrusion nozzle, respectively. The diameter of the extruded filament can be controlled by changing the extrusion nozzle diameter and/or the rotation speed of the mandrel. If the mandrel rotation speed is high enough to stretch the extruded filament, it will decrease its diameter. The printed helical structure can be taken off from the mandrel manually by pulling the microcoil out of the rod after the solidification of polymer.

The advantage of this method compared to the UV- and SC-3D printing methods previously discussed in this review is the higher

precision on the diameter and also the pitch of the helical structure. These advantages basically originate from the fact that the extruded ink is entirely supported by the mandrel, which mostly removes the influence of the gravity on the deformation of the helical structure during its solidification. The main drawback of this method compared to other 3D printing methods is its limitation on the shape of the printed structure, as the printed structure should be taken off the mandrel after its fabrication. A fabrication tolerance of 1-3% was reported by Lanouette et al. using PLA/DCM solution with a concentration of 30 wt.%.<sup>52</sup> Their printed helical shaped PLA was coated with copper for the creation of a micro-antenna. Figure 8c shows optical images of the variable pitches micro-antenna. The antenna was fabricated using 30 wt.% PLA solution and the micronozzle with the ID of 200  $\mu\text{m}$  and an extrusion pressure of 2.8 MPa while the rotational speed varied to obtain different pitches. The diameter of the coil is  $\sim 4$  mm and its height is  $\sim 21$  mm with the filament's diameter of  $\sim 200$   $\mu\text{m}$ .

## Applications

### 1. MEMS and NEMS: mechanical microsprings, strain/load sensors and flow sensor, mechanical switch and electrostatic actuator

Microactuators and microsensors with the ability to sense their environments are important types of MEMS. Their miniaturized size in most cases enable them for faster and more reliable results compared to larger actuators or sensors. The efficiency and reliability of such microsystems depend on the materials used as sensing elements as well as the optimization of the component geometry. With their unique geometry, helical microstructures have been demonstrated as efficient potential components for 3D MEMS. Lebel et al. reported the fabrication of a nanocomposite helical structure network which could be integrated into MEMS due to their load bearing capability.<sup>25</sup> Figure 9a shows a SEM image of the mechanical microsprings network in a triangle layout fabricated using the UV-3DP technique. The microcoils were composed of 6 turns having a pitch of 1 mm and flat film and last coils with the total height of 5 mm. The material used was the UV-curable urethane-based (NEA123MB) nanocomposite containing 0.5 wt.% carbon nanotubes and 1 wt.% silica particles. Mechanical testing of the network under compression showed a quasi-linear response with a network rigidity of  $\sim 11.7$  mN mm<sup>-1</sup>. The mechanical properties of these microsprings could be controlled by using other materials and changing the geometry characteristics of the coils.

Nanocomposite helical microstructures have also been demonstrated as a 3D strain sensor.<sup>11</sup> Figure 9b shows a SEM image of the 3D sensor which composed of a network of four identical microcoils in a square layout. The helical microcoils with seven 1 mm-diameter turns and inter-coil distance of 3 mm were fabricated through UV-3DP of UV-curable epoxy nanocomposites containing 1 wt.% of single-walled carbon nanotubes. The height of microcoils was  $\sim 6$  mm and the filament's diameter was  $\sim 150$   $\mu\text{m}$ . In carbon nanotube-based nanocomposite sensors with two-dimensional (2D) or 3D geometries, the electrical conductivity is based on the formation of percolation pathways of carbon nanotubes. The deformation induced by an external mechanical force can change the arrangement of the conductive nanofillers leading to a variation in the electrical conductivity of the nanocomposite.<sup>53</sup> 2D nanocomposite films have been extensively studied in the literature as high-sensitive strain sensors for structural health monitoring.<sup>54</sup> Nanocomposite films only provide in-plane strain measurements due to their planar geometry. Moreover, capturing

undesired stimulus might result in unreliable measurements as the film sensor must be in contact with the structure in its whole surface area.<sup>55</sup> In addition to be capable of sensing out-of-plane strains, the 3D sensor may overcome the issues related to the nanocomposite 2D films while offering higher electromechanical sensitivity (e.g., gauge factor of 3.2) when compared to traditional strain gauges (e.g., gauge factor of  $\sim 2$ ). The helical geometry of this sensor enables the electromechanical measurement both in tension and compression and also allows large displacement. The mechanical behavior of these helical sensing components could be tailored by their geometry and/or material used. This 3D nanocomposite sensor may have high potential for novel instrumentation approaches due to its high sensitivity, compactness, lightness and other unique features such as flexibility and feasibility of the direct printing of sensing elements onto the structure.

3D nanocomposite helical microstructure, either individually or in a network, may also have potential as high-efficient liquid and flow sensors.<sup>56, 57</sup> Figure 9c shows a SEM image of an individual microcoil having 5 turns while the fabrication of the last coil continued over an aluminum block which was used as an electrode for electrical measurement. The structure shown in Figure 9c were fabricated using UV-curable urethane-based (NEA123MB) nanocomposite containing 0.5 wt.% carbon nanotubes and 5 wt.% silica particles. Such sensors have the potential to accurately sense various solutions (e.g., solvents,<sup>58</sup> biomaterials solution<sup>59</sup>) and/or a stream of flow (e.g., flow rate<sup>56, 60</sup>) by monitoring the variation of their electrical conductivities which are highly sensitive to small chemical and mechanical disturbances. Similar to the electromechanical resistivity of nanocomposites, the same mechanism can be used to interpret the electrochemical sensitivity. When the nanocomposite coils are surrounded by a chemical, the nanocomposite filaments may experience expansion (swelling) or contraction (shrinkage). Both changes cause a re-arrangement of conductive nanofillers in their percolation pathways. The 3D feature of these sensors offers a high surface area and mechanical flexibility.

Mutsui et al. reported the fabrication of a mechanical switch using FIB-CVD.<sup>27</sup> Figure 9d schematically represents the switch and its working mechanism. Figure 9e-f shows the structured illumination microscopy (SIM) images of the fabricated switch before and after applying voltage. The device composed of a helical coil and free-space nanowiring fabricated onto the Au electrodes. Applying opposite electrical charges to the wiring and the coil resulted in the formation of repulsive forces between each coil's turn and subsequently the coil extended upward until contacted the wiring. The author mentioned that the switch working functions are the voltage of 30 V which corresponded to a pulsed current of about 170 nA. They also demonstrated the application of helical structures as electrostatic actuator. Figure 9g-h shows SIM image of the electrostatic actuator and its working principle, respectively. This device was fabricated on the tip of a Au-coated glass capillary using the FIB-CVD technique at a current of 7 pA and an exposure time of 10 min. The working mechanism of the device is based on the formation of repulsive forces as a result of electric charge accumulation through which leads to the coil expansion. The coil can store electric charge when a voltage is applied across the glass capillary. The magnitude of coil expansion depends on the applied voltage.<sup>27</sup>

### 2. Lab-on-a-chip systems: cell separators

High efficient lab-on-a-chip systems, specifically those used for the detection and separation of microparticles such as cells and

viruses, have rapidly progressed through the miniaturization of components and the fabrication of smaller functional devices.<sup>63</sup> The miniaturization of these systems via the design and fabrication of complex 3D microfluidic devices showed new functionality and increased performance.<sup>61, 62</sup> Helical geometries have been recently used in the fabrication of high-efficiency dielectrophoretic (DEP) cell separators in two different avenues: helical-shaped microelectrodes and helical-shaped microfluidic channels.<sup>64</sup> The first presented device comprises of 378 interdigitated microelectrodes that induce non-uniform electric field as driving forces for cell separation. Figure 10a shows an optical image of a fabricated microdevice composed of 30 gold-sputtered 3D helical interdigitated microelectrodes and Figure 10b shows its side view. Figure 10c shows a top-view image of the 3D electrodes (gold-sputtered components). The fabrication of the device began with the deposition of a sacrificial ink filament in a 2D square-wave feature (10 turns). Thirty microcoils (3 for each interdigitated electrode) having turns with the coil diameter of 1 mm, the pitch of 0.5 mm, and a filament diameter of 100  $\mu\text{m}$  were then deposited inside the ink filaments through the UV-3DP of the UV-curable urethane-based resin (NEA123T). The whole structure was then gold-sputtered to create a conductive layer of 120  $\mu\text{m}$ . The sacrificial 2D ink filaments were finally removed from the device using hexane to create the gap between two electrodes. Figure 10d schematically represents the particles (blue and red) separation through dielectrophoresis when passing through two neighboring helical electrodes. The particles used in this study were polystyrene microbeads of 4 and 10  $\mu\text{m}$  diameter.<sup>62</sup> Compared to its associated 2D counterpart, the 3D microelectrode showed highly efficient particle separation with  $\sim 50\%$  and  $\sim 700\%$  improvement in the separation efficiency and capacity, respectively. The separation efficiency is based on the magnitude and orientation of the DEP forces which depend on different parameters including the electric field gradient. The shape complexity provided by the 3D helical microcoils enabled the creation of inhomogeneity of the electric field, increasing separation efficiency. Therefore, the non-uniform electric field and high surface area provided by the helical electrodes are thought to be responsible for the higher efficiency of the device when compared to the 2D counterpart. A further study may be required to investigate different geometries (e.g., arrays of vertical filaments) to find the best 3D feature that provides the highest separation efficiency. Lab-on-a-chip systems composed of 2D and 3D microfluidic channels have been mostly fabricated using conventional photolithography techniques. However, newly-developed techniques based on laser irradiation<sup>14, 15</sup> and 3D printing enabled the facile fabrication of 3D microchannels for high complex microfluidic systems. The second device shown in Figure 11 is a 3D helical-shaped microfluidic cell separator consisting of two helical microchannels, fabricated using CPM 3D printing. Figure 11a shows a scheme of the 3D particles separation composed of two helical microchannels and three reservoirs: mixed particles reservoir, and two reservoirs to gather separated particles. In this device, the particle separation is based on insulator-based dielectrophoresis (iDEP). The helical microfluidic channels are non-conductive (i.e., the electrodes are outside of channels) and the non-uniformity of the electric field comes from the shape of the device. The first helical microchannel featuring constant clockwise turns is responsible for aligning all particles along the outside wall. When aligned, particles entered the second helical microchannel featuring counter-clockwise turns, they are placed in its inside wall.

Similarly, the electric field gradient pushes more the larger particles than the smaller ones. The shorter travelling distance along the second channel enables the separation at Y joint before the particles move to the outside of the second helical channel. The authors believe that the manufactured 3D helical microfluidic channels offer constant curvature radius that generates a constant electric field gradient which cannot be achieved in 2D spiral-shaped separators.

The channels were fabricated by first depositing a sacrificial ink on rotating 1.2 mm diameter mandrels to create two helices with numbers of coils of 6 and 4, respectively. The sacrificial ink was a binary mixture of a microcrystalline wax (Strahl & Pitsch, USA) and a petroleum jelly (Unilever, Canada) with a weight proportion of 30:70. The mandrel and the helices were then encapsulated using a two-part liquid epoxy resin (Epon 862 / Epikure 3274, Momentive, USA). Upon curing of epoxy at room temperature for 48 h, the entire device was heated in boiling water and the ink was removed upon its liquefaction by applying vacuum to one end of the ink helical structure resulting the formation of helical microchannels. Figure 11b is an inset of Figure 11a that schematically represents the particles separation at Y junction through dielectrophoresis forces. Figure 11c shows an optical image of the fabricated separator and Figures 11d-f show fluorescent images of the helical channels, the Y junction, and slightly inclined bottom view of the separator, respectively. To evaluate the separation efficiency, a particle suspension containing 4  $\mu\text{m}$  and 6  $\mu\text{m}$  polystyrene microbeads in an aqueous solution of sodium chloride was used. A particle separation efficiency of 94% was obtained by applying a voltage of 900 VDC. Although the efficiency reported in the work is similar to the 2D separators, it could be optimized by possibly tailoring of the number of turns for each helix. In planar (2D) spiral devices, the force applied on a given particle is inversely proportional to the curvature radius of the channel. For an efficient separation in 2D configurations, longer channels should be used, leading to larger curvature radius and consequently lower separating forces. One of the main advantages of the helical microchannel device over, for instance, a planar spiral device is that in a helical channel the curvature radius is constant, thus resulting in constant separation forces (as a result of a constant electric field gradient) throughout the channel regardless of its length. Both works presented in this section show an original utilization of the helical microstructure and the potential to build a real lab-on-a-chip device for biocells separation (e.g., cancer cell detection). The main advantage of the helical microfluidic cell separator over the 3D interdigitated electrode separator may be the possibility of keeping the electrodes away from the separation site that helps minimizing the issues related to Joule heating and electrolysis. The fabrication of such complex 3D microdevices opens avenues to miniaturize lab-on-a-chip systems with high efficiency and thus, make them portable and affordable.<sup>64</sup>

### 3. Microelectronics and telecommunications

Helical structures have shown several potential applications in the field of microelectronics and telecommunications due to their unique shape. Their spring shape makes them good candidates as the interconnections in stretchable and/or flexible electrical circuits. Unlike the filaments that can break while stretching, helical structures have the capability to adapt their height to the deformation applied to the system in a specific direction. The helical structures can also be used as inductors. A metallic coil wrapped around a magnetic core, usually made of iron or ferrite, can be used as a generator of magnetic field. In the field of



telecommunication helical structures are widely used antennas. Due to the increasing constraints on the size and performance of electronic and telecommunication devices, advanced fabrication methods and materials must be developed to answer the industrial needs.

Recently three different methods have been reported for direct writing of metal wires such as extrusion of metal particles from a nozzle,<sup>65</sup> by electrodeposition from a conductive tip<sup>48</sup> or 3D printing of freeform liquid metal.<sup>66</sup> These fabrication methods can open a new pathway toward construction of microelectronics such as 3D or flexible electrical circuits. Printed electronics such as electrical components suitable for radio-frequency identification (RFID) or pMOS and nMOS transistors have been reported by Subramanian et al.<sup>67</sup> In this later work it is demonstrated that transistors components can be made by printing of various novel organic semiconductors, dielectrics and nanoparticle-based conductors. Lanouette et al. have shown the possibility of fabricating helical micro-antenna arrays using the 3D conformal printing of PLA/DCM on rotating mandrels followed by coating the helices with a thin layer of copper (Figure 12a).<sup>52</sup> These micro-antennas operate in the Ka band (i.e., 20–30 GHz) showing their potential as high frequency band antennas. The geometry of the helical structure defines the electrical parameters of the antenna (i.e. receiving and transmitting frequencies, gain, axial ratio, etc.). The helical shape provides a circular polarization with a relatively high gain regarding the size of the antenna. These micro-antennas have variable pitches which allow them to work in two distinct frequency bands (uplink frequencies range from 30.0 to 31.93 GHz and downlink from 20.2 to 21.2 GHz) and thus one micro-antenna can be used as a receiver and transmitter. The size of the helix (i.e. diameter of the helix and of the filament) is inverse proportional to its operating frequencies.

In another work, Adams et al. reported the fabrication of small antennas onto either the exterior or interior surface of a hollow glass hemisphere in the form of conductive meander lines (Figure 12b).<sup>68</sup> The method used for the construction of these antennas was conformal printing of a concentrated silver nanoparticle ink onto convex and concave hemispherical surfaces. Four small antennas of varying Ka, operating frequency and meander line size were made demonstrating different possible 3D antenna designs other than the helical shape.

## Concluding remarks, challenges and future opportunities

The technology of 3D printing is rapidly growing due to the ease of use and variety of the application fields. Wide diversity of shapes can be modeled by different software and printed by 3D printers. Among the different shapes and structures made by various 3D printing methods, helical forms have attracted the attention of researchers due to their potential in different applications such as drag control in aircraft, beam focusing and steering, microsensing devices, electromagnetic shielding, micro-antennas, stretchable/flexible microelectronics, liquid gas sensors, MEMS and lab-on-a-chips. Various types of 3D printing methods (i.e., FIB-CVD, MSL, MCED, UV-3DP, 3DP, CPRM and FDM) are suitable for the fabrication of helical microstructures.

Despite the progresses that have been made in the field of 3D printing, there are some limitations with respect to the size, material and complexity of the helical structures to be printed. Among the techniques discussed in the review paper, MSL and FIB-CVD are capable of printing helical structures with a resolution down to submicron, however they are costly and

require very expensive equipment. The limitation on the size regarding the freeform 3D printing based on robotic direct deposition of inks filament generally comes from the resolution of the 3D printing robots, the nozzle size and printability of different materials from the nozzles with certain sizes. The evolution of making the robots featuring higher precision of moving in different directions is going to improve the resolution of 3D printers. The advances on the fabrication of nozzles with fine sizes such as 1  $\mu\text{m}$  can also help decreasing the size of extruded filaments leading to printing the helical microstructures with smaller filament diameters. On the other hand, submicron-size structures have also been made using the two-photon polymerization method<sup>69</sup>. One of the main challenges that limits the capability of helical microstructure fabrication by 3D printing method is the limitation on the type of the printable materials. The most commonly used materials so far are the polymers as their transformation from solid-like to fluid-like and inverse is easier compared to other types of materials such as metals and ceramics. Printing of ceramic or metal loaded polymers have been also reported which were the first steps toward 3D printing of ceramic and metallic helical structures.<sup>40</sup> Recently the possibility of freeform 3D printing of liquid metals has been shown which can facilitate the printing different types of structures useful for microelectronics.<sup>66</sup> These progresses in fabrication of 3D printing robots with high resolution, nozzles with very fine sizes and variety of printable materials show a promising pathway toward 3D printing of helical microstructures with higher resolutions and smaller sizes.

## Acknowledgments

The authors acknowledge the financial support from Natural Sciences and Engineering Research Council of Canada (NSERC) and Canada Research Chair on Fabrication of microsystems and advanced materials. The authors would like to thank all members of Laboratory for Multiscale Mechanics (LM<sup>2</sup>) research group at École Polytechnique de Montréal, especially Dr. Louis Laberge Lebel, Dr. Hamid Dalir, Mr. Shuangzhan Guo, Ms. Anne-Marie Lanouette and Mr. Nicolas Guerin for their assistance to gather some required information.

## Note

Author's affiliation:

Laboratory for Multiscale Mechanics (LM<sup>2</sup>), Department of Mechanical Engineering, École Polytechnique de Montréal, C.P. 6079, Succ. Centre-ville, Montréal, QC H3C 3A7, CANADA.

\* Corresponding author:

Phone: 1 (514) 340-4711 (ext. 4419)

E-mail address: [daniel.therriault@polymtl.ca](mailto:daniel.therriault@polymtl.ca)

## References

1. M. Cima, E. Sachs, L. Cima, J. Yoo, S. Khanuja, S. Borland, B. Wu and R. Giordano, *Solid Freeform Fabr. Symp. Proc.*, 1994, 181–190.
2. B. Utela, D. Storti, R. Anderson and M. Ganter, *Journal of Manufacturing Processes*, 2008, **10**, 96–104.
3. B. Khoshnevis, *Automation in Construction*, 2004, **13**, 5–19.
4. S. Kawata, H.-B. Sun, T. Tanaka and K. Takada, *Nature*, 2001, **412**, 697–698.
5. K. Leong, C. Cheah and C. Chua, *Biomaterials*, 2003, **24**, 2363–2378.

- 1 6. <http://www.designboom.com/technology/nanoscribe-nanoscale-3d-printed-microstructures/>, 2013.
- 2 7. C. Ladd, J. H. So, J. Muth and M. D. Dickey, *Advanced materials*, 2013, **25**, 5081-5085.
- 3 8. J. D. Pitts, P. J. Campagnola, G. A. Epling and S. Goodman, *Macromolecules*, 2000, **33**, 1514-1523.
- 4 9. R. Engelke, G. Engelmann, G. Gruetzner, M. Heinrich, Kubenz and H. Mischke, *Microelectron Eng*, 2004, **73**, 456-462.
- 5 10. A. R. Djordjevic, A. G. Zajic, M. M. Ilic and G. L. Stuber, *Antennas and Propagation Magazine, IEEE*, 2006, **48**, 115.
- 6 11. R. D. Farahani, H. Dalir, V. Le Borgne, L. A. Gautier, A. El Khakani, M. Levesque and D. Therriault, *Nanotechnology*, 2012, **23**, 085502.
- 7 12. V. K. Varadan, V. V. Varadan and S. Motojima, *Photo-Opt Ins*, 1996, **2722**, 156-164.
- 8 13. M. Feldmann, A. Waldschik and S. Biittgenbach, *Microelectronics: Design, Technology, and Packaging*, 2008, **6798**, 79811.
- 9 14. S. G. He, F. Chen, K. Y. Liu, Q. Yang, H. W. Liu, H. Bian, X. W. Meng, C. Shan, J. H. Si, Y. L. Zhao and X. Hou, *Lett*, 2012, **37**, 3825-3827.
- 10 15. S. G. He, F. Chen, Q. Yang, K. Y. Liu, C. Shan, H. Bian, W. Liu, X. W. Meng, J. H. Si, Y. L. Zhao and X. Hou, *Micromech Microeng*, 2012, **22**, 105017.
- 11 16. Y. B. Huang, L. Y. He, H. Y. Jiang and Y. X. Chen, *In Mol Sci*, 2012, **13**, 6849-6862.
- 12 17. R. N. Dean, P. C. Nordine and C. G. Christodoulou, *Terahertz Spectroscopy and Applications*, 1999, **3617**, 77.
- 13 18. R. N. Dean, P. C. Nordine and C. G. Christodoulou, *Opt Techn Lett*, 2000, **24**, 106-111.
- 14 19. A. Khaleghi, A. Azoulay and J. C. Bolomey, *Wireless Commun*, 2009, **50**, 417-434.
- 15 20. M. J. Wilhelm, R. M. Taylor and R. T. Salisbury, *US Patent*, 2007, **7183998**.
- 16 21. A. Yamada, F. Niikura and K. Ikuta, *J Micromech Microeng*, 2008, **18**, 025035.
- 17 22. S. Kawata, H. B. Sun, T. Tanaka and K. Takada, *Nature*, 2001, **412**, 697-698.
- 18 23. L. Kelemen, P. Ormos and G. Vizsniczai, *Journal of European Optical Society-Rapid publications*, 2011, **11029**.
- 19 24. S. Z. Guo, F. Gosselin, N. Guerin, A. M. Lanouette, M. Heuzey and D. Therriault, *Small*, 2013, **4118-4122**.
- 20 25. L. L. Lebel, B. Aissa, M. A. El Khakani and D. Therriault, *Advanced materials*, 2010, **22**, 592-596.
- 21 26. B. Jia, L. Yu, F. Fu, L. Li, J. Zhou and L. Zhang, *Advances*, 2014.
- 22 27. S. Matsui, in *Springer Handbook of Nanotechnology*, Springer, 2010, pp. 211-229.
- 23 28. S. Reyntjens and R. Puers, *J Micromech Microeng*, 2010, **10**, 181.
- 24 29. S. Matsui, T. Kaito, J.-i. Fujita, M. Komuro, K. Kanda, Y. Haruyama, *Journal of Vacuum Science & Technology*, 2000, **18**, 3181-3184.
- 25 30. J.-W. Choi, R. B. Wicker, S.-H. Cho, C.-S. Ha and S. Lee, *Rapid Prototyping Journal*, 2009, **15**, 59-70.
- 26 31. D. Therriault, R. F. Shepherd, S. R. White and J. A. Lewis, *Advanced materials*, 2005, **17**, 395-399.
- 27 32. D. Therriault, S. R. White and J. A. Lewis, *Nat Mater*, 2005, **4**, 347-347.
- 28 33. D. Therriault, S. R. White and J. A. Lewis, *Appl Rheol*, 2007, **17**, 10112.
- 29 34. G. M. Gratson and J. A. Lewis, *Langmuir*, 2005, **21**, 457-464.
- 30 35. G. M. Gratson, M. J. Xu and J. A. Lewis, *Nature*, 2004, **428**, 386-386.
- 31 36. J. E. Smay, G. M. Gratson, R. F. Shepherd, J. Cesarano and J. A. Lewis, *Advanced materials*, 2002, **14**, 1279-1283.
- 32 37. S. Z. Guo, M. C. Heuzey and D. Therriault, *Langmuir*, 2014, **30**, 1142-1150.
- 33 38. R. D. Farahani, L. L. Lebel and D. Therriault, *Accepted in Journal of Micromechanics and Microengineering*, 2013.
- 34 39. A. Tsouknidas, *Advances in Tribology*, 2011, **2011**, 746270.
- 35 40. M. Allahverdi, S. C. Danforth, M. Jafari and A. Safari, *J Eur Ceram Soc*, 2001, **21**, 1485-1490.
- 36 41. S. Crump, *US Patent*, 1992, 5121329 A.
- 37 42. A. Safari, *Ferroelectrics*, 2001, **263**, 1345-1354.
- 38 43. C. S. Lee, S. G. Kim, H. J. Kim and S. H. Ahn, *J. Mater. Process. Technol.*, 2007, **187-188**, 627-630.
- 39 44. M. McGurk, A. A. Amis, P. Potamianos and N. M. Goodger, *Annals of the Royal College of Surgeons of England*, 1997, **79**, 169-174.
- 40 45. S. Kumar and J. P. Kruth, *Materials & Design*, 2010, **31**, 850-856.
- 41 46. J. E. Rabinovich, *US Patent: 5578227*, 1998.
- 42 47. <http://www.3ders.org/pricecompare/3dprinters/>.
- 43 48. J. Hu and M.-F. Yu, *Science*, 2010, **329**, 313-316.
- 44 49. <http://gallery.mailchimp.com/dc5612c382e7ffe99c7571e3f/files/Nanomanufacturing.pdf>, 2010.
- 45 50. C. Decker, *Prog Polym Sci*, 1996, **21**, 593-650.
- 46 51. Z.-M. Huang, Y.-Z. Zhang, M. Kotaki and S. Ramakrishna, *Compos. Sci. Technol.*, 2003, **63**, 2223-2253.
- 47 52. A. Lanouette, J. Hill, P. Dussault, J. Laurin and D. Therriault, *Nanotech*, 2013, **2**, 416-419.
- 48 53. N. Hu, Y. Karube, C. Yan, Z. Masuda and H. Fukunaga, *Acta Mater*, 2008, **56**, 2929-2936.
- 49 54. G. Yin, N. Hu, Y. Karube, Y. L. Liu, Y. Li and H. Fukunaga, *J Compos Mater*, 2011, **45**, 1315-1323.
- 50 55. P. Murugaraj, D. E. Mainwaring and N. Mora-Huertas, *Compos Sci Technol*, 2009, **69**, 2454-2459.
- 51 56. H. Cao, Z. Y. Gan, Q. Lv, H. Yan, X. B. Luo, X. H. Song and S. Liu, *Microsyst Technol*, 2010, **16**, 955-959.
- 52 57. J. Choi and J. Kim, *Nanotechnology*, 2010, **21**, 105502.
- 53 58. M. Penza, G. Cassano, P. Aversa, F. Antolini, A. Cusano, M. Consales, M. Giordano and L. Nicolais, *Ieee Sensor*, 2004, 403-406.
- 54 59. B. N. Wang, J. B. Zheng, Y. P. He and Q. L. Sheng, *Sensor Actuat B-Chem*, 2013, **186**, 417-422.
- 55 60. Y. Ito, T. Higuchi and K. Takahashi, *J Therm Sci Tech-Jpn*, 2010, **5**, 51-60.
- 56 61. D. F. Chen, H. Du and W. H. Li, *J Micromech Microeng*, 2006, **16**, 1162-1169.
- 57 62. H. Dalir, R. D. Farahani, L. Hernandez, C. Aldebert, M. Levesque and D. Therriault, *Submitted to journal of Small*, 2013, 21.
- 58 63. K. Khoshmanesh, C. Zhang, F. J. Tovar-Lopez, S. Nahavandi, S. Baratchi, A. Mitchell and K. Kalantar-Zadeh, *Microfluid Nanofluid*, 2010, **9**, 411-426.
- 59 64. N. Guerin, M. Lévesque and D. Therriault, *Accepted in Journal of Biomedical Science and Engineering (JBSE)*, 2014.
- 60 65. B. Y. Ahn, E. B. Duoss, M. J. Motala, X. Guo, S.-I. Park, Y. Xiong, J. Yoon, R. G. Nuzzo, J. A. Rogers and J. A. Lewis, *Science*, 2009, **323**, 1590-1593.

- 1 66. C. Ladd, J.-H. So, J. Muth and M. D. Dickey, *Adv. Mater.*,  
2 2013, **25**, 5081-5085.
- 3 67. V. Subramanian, J. M. J. Frechet, P. C. Chang, D. C. Huang,  
4 J. B. Lee, S. E. Molesa, A. R. Murphy, D. R. Redinger and  
5 S. K. Volkman, *Proceedings of the IEEE*, 2005, **93**, 1330-  
6 1338.
- 7 68. J. J. Adams, E. B. Duoss, T. F. Malkowski, M. J. Motala, B.  
8 Y. Ahn, R. G. Nuzzo, J. T. Bernhard and J. A. Lewis, *Adv.*  
9 *Mater.*, 2011, **23**, 1335-1340.
- 10 69. M. Thiel, M. S. Rill, G. von Freymann and M. Wegener,  
11 *Adv. Mater.*, 2009, **21**, 4680-4682.
- 12 70. B. Y. Ahn, E. B. Duoss, M. J. Motala, X. Y. Guo, S. I. Park,  
13 Y. J. Xiong, J. Yoon, R. G. Nuzzo, J. A. Rogers and J. A.  
14 Lewis, *Science*, 2009, **323**, 1590-1593.
- 15 71. M. Woytasik, J.-P. Grandchamp, E. Dufour-Gergam, J.-P.  
16 Gilles, S. Megherbi, E. Martincic, H. Mathias and P. Crozat,  
17 *Sensors and Actuators A: Physical*, 2006, **132**, 2-7.
- 18 72. J. D. Madden and I. W. Hunter, *J Microelectromech S*,  
19 1996, **5**, 24-32.
- 20 73. H.-P. Chang, J. Qian, M. Bachman, P. Congdon and G.-p.  
21 Li, *SPIE's 9th Annual International Symposium on Smart*  
22 *Structures and Materials*, 2002, 187-195.

23

24

## ARTICLE

## Tables and Figures

Table 1. Selected microfabrication techniques capable of 3D freeform fabrication

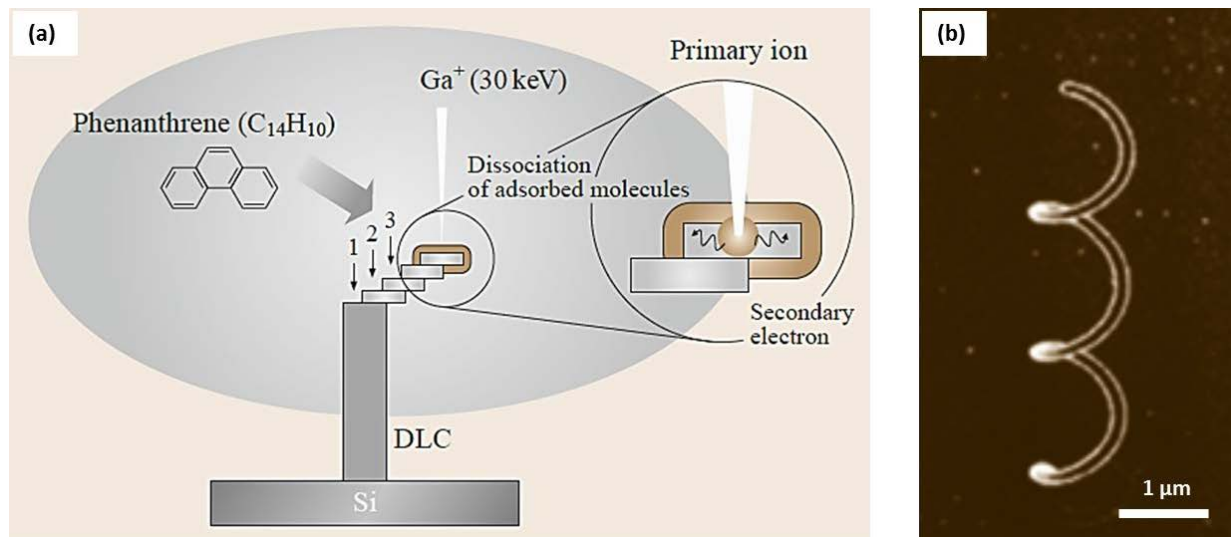
Technique	Material used	Minimum feature size	Creation of helical structures	Refs
Two-photon polymerization	Photopolymers (Urethane acrylate)	Down to 120 nm	No	22
<b>Focused ion beam chemical vapor deposition (FIB-CVD)</b>	Gaseous reactants (Phenanthrene)	Down to few hundred nm	Yes	27, 28
Multi-photon polymerization	Photopolymers (Acrylic) Photopolymers (Proteins)	Submicron Submicron	No No	23 8
Direct deposition of metals	Metal inks Liquid metals	Down to 2 $\mu\text{m}$ Down to 10 $\mu\text{m}$	No No	70 7
<b>Meniscus-confined electrodeposition (MCEP)</b>	Electrolyte (metals solution)	Down to 2 $\mu\text{m}$	Yes	48
<b>Microstereolithography</b>	Photopolymers and photoabsorbers	Down to 25 $\mu\text{m}$	Yes	12, 30
Laser chemical vapor deposition	Gaseous reactants	Down to 40 $\mu\text{m}$	No	18
<b>Fused deposition modeling (FDM)</b>	Thermoplastics (Poly lactic acid)	Down to 45 $\mu\text{m}$	Yes	21
<b>UV-3D printing (UV-3DP)</b>	Photopolymers (Urethane, epoxy)	Down to 100 $\mu\text{m}$	Yes	11, 25
<b>Solvent-cast 3D printing (SC-3DP)</b>	Thermoplastics (PLA)	Down to 150 $\mu\text{m}$	Yes	24
<b>Conformal printing on rotating mandrel (CPRM)</b>	Thermoplastics (PLA)	Down to 200 $\mu\text{m}$	Yes	52
Photolithography	Photopolymers (PMMA)	Few hundreds microns	No	71
Localized electrochemical Deposition	Metals (Nickel)	1 mm	No	72
UV depth lithography	Photopolymers (SU-8 AZ9260, Intervia-3D-N and CAR44)	Few millimeters	No	13
Compressive molding planarization	Metals (Copper)	Millimeters	No	73

Table 2. Examples of materials used for the fabrication of 3D helical microstructures by UV-3DP.

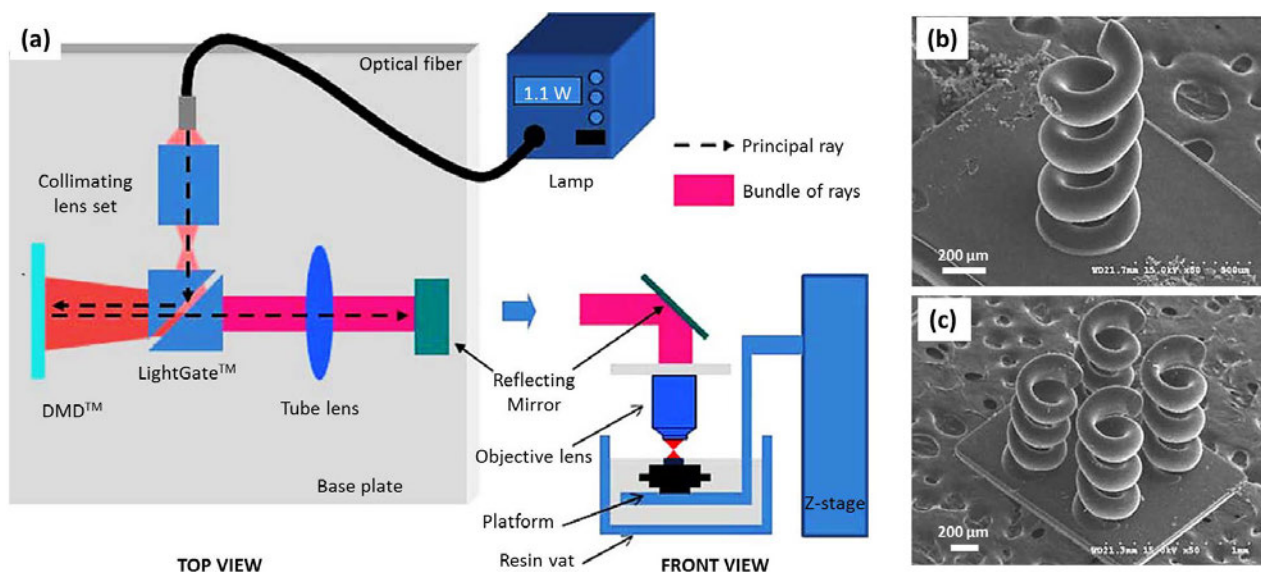
Material	Product name	Nanofiller	Weight fraction (%)	Viscosity (Pa.s)	Ref.
Urethane-based	NEA 123T, Norland Products Inc.	-	-	250	38
	NEA 123MB, Norland Products Inc.	Silica particles	5	100	25
		Carbon nanotubes Silica particles	0.5 5	230	25
		Carbon nanotubes Silica particles	1 5	300	25
		Carbon nanotubes	0.5	90	38
Epoxy-based	UV-DC80, Master bonds	Carbon nanotubes	1	160	38
		Carbon nanotubes	1	160	38

Table 3. Summary table showing the advantages, limitations and potential applications of the different 3D printing techniques.

Technique Fabrication mechanism	Pros	Cons	Selected potential application
<b>FIB-CVD</b> Localized chemical vapor deposition using focused ion beam in a vacuum chamber	High fabrication resolution (down to ~100 nm)	Expensive equipment  Limited material selection  Requires high vacuum environment	MEMS and NEMS: electrostatic actuators  Microelectronics  Nanomechanical switch
<b>MSL</b> Solidification of photopolymers upon curing under the focused UV light by controlling its penetration into the resin	Very mature knowledge database due to its long usage history  Capability of producing microstructures with the part volume of a few millimeters and the smallest feature of a few microns	Expensive equipment  Limited material selection: requires low viscosity materials  Needs additional equipment and materials (e.g., mask, photoabsorber)	Drag control in aircraft  Beam focusing and steering  Electromagnetic shielding and absorption
<b>FDM</b> Solidification of molten thermoplastic materials upon cooling by air shortly after exiting the extrusion nozzle	Diversity of materials used  Advanced ink feeding system  Very mature knowledge database due to its long usage history	High energy consumption as it works at high temperatures  Incompatible with the materials that degrade at high temperatures  Possible processing difficulties due to working with viscos materials	3D printing of most of the structures ranging from millimeter and higher scales  Tissue engineering by the utilization of biocompatible PLA  Liquid sensor by the polymer swelling with a solvent
<b>MCED</b> Electrodeposition of metals in an electrolyte solution using the thermodynamic stability of a liquid meniscus	Capable of fabricating nano- and microstructures  Very precise metal deposition at room temperature  Relatively low fabrication and tooling costs	Limited by material constraints: metals those can be electrochemically deposited  Requires highly calibration of the parameters to form meniscus	High density interconnects for integrated circuits  High aspect ratio AFM probes for critical metrology  Nanoscale needle probes or probe arrays
<b>UV-3DP</b> Solidification of UV-curable thermosetting materials upon fast curing under the UV exposure shortly after exiting the extrusion nozzle	Suitable for freeform 3D printings at room temperature  No need for toxic solvents  Use of materials with low to moderate viscosities: facile processing	Needs user caution and proper protection: working with UV light  Not suitable for low viscosity Newtonian materials  Needs high materials curing reactivity	MEMS components: displacement sensor,  Lab-on-a-chip systems: cell separator  Electromagnetic interference (EMI) shielding, Flexible microelectronics
<b>SC-3DP</b> Solidification of thermoplastic polymer solution upon fast solvent evaporation shortly after exiting the extrusion nozzle	Suitable for freeform 3D printings at room temperature  Low deformation of the structure during solidification	Use of toxic solvent  Limited to highly volatile solvent for fast evaporation	MEMS components: Liquid sensor and high stiffness/conductive MEMS
<b>CPRM</b> Extrusion of filament around a rotating mandrel	Very precise fabrication method  Diversity of the materials used Simplicity of the technique  Capable of fabricating high aspect ratio (length/diameter) structures	Limited to simple geometries  Possible difficulties regarding taking off the printed object from the mandrel	Microelectronics: Antennas Lab-on-a-chip systems: microchannel cell separator



**Figure 1.** FIB-CVD fabrication of freeform helical structures: (a) schematic representation of the technique and a conventional set-up with  $\text{Ga}^+$  ions and Phenanthrene as precursor gas, and (b) image of a helical structure having 3 turns with a coil diameter of  $0.6 \mu\text{m}$ , a coil pitch of  $0.7 \mu\text{m}$  and a filament diameter of  $0.08 \mu\text{m}$  fabricated using a  $\text{Ga}^+$  ion beam and a phenanthrene as precursor gas and nozzle's internal diameter of  $0.3 \text{ mm}$ .<sup>27</sup>



**Figure 2.** MSL fabrication of freeform helical microstructures: (a) schematic representation of the technique with a usual set-up, (b) and (c) SEM images of helical structures (individual or network) with the coil's diameter of  $500 \mu\text{m}$  and the filament's diameter of  $130 \mu\text{m}$ . The exposure energy of  $33.8 \text{ mJ/cm}^2$  and an acrylate-based commercial resin mixed with 5 wt.% of a photoinitiator and 0.15 wt.% Tinuvin 327™ as the photoabsorber were used.<sup>30</sup>



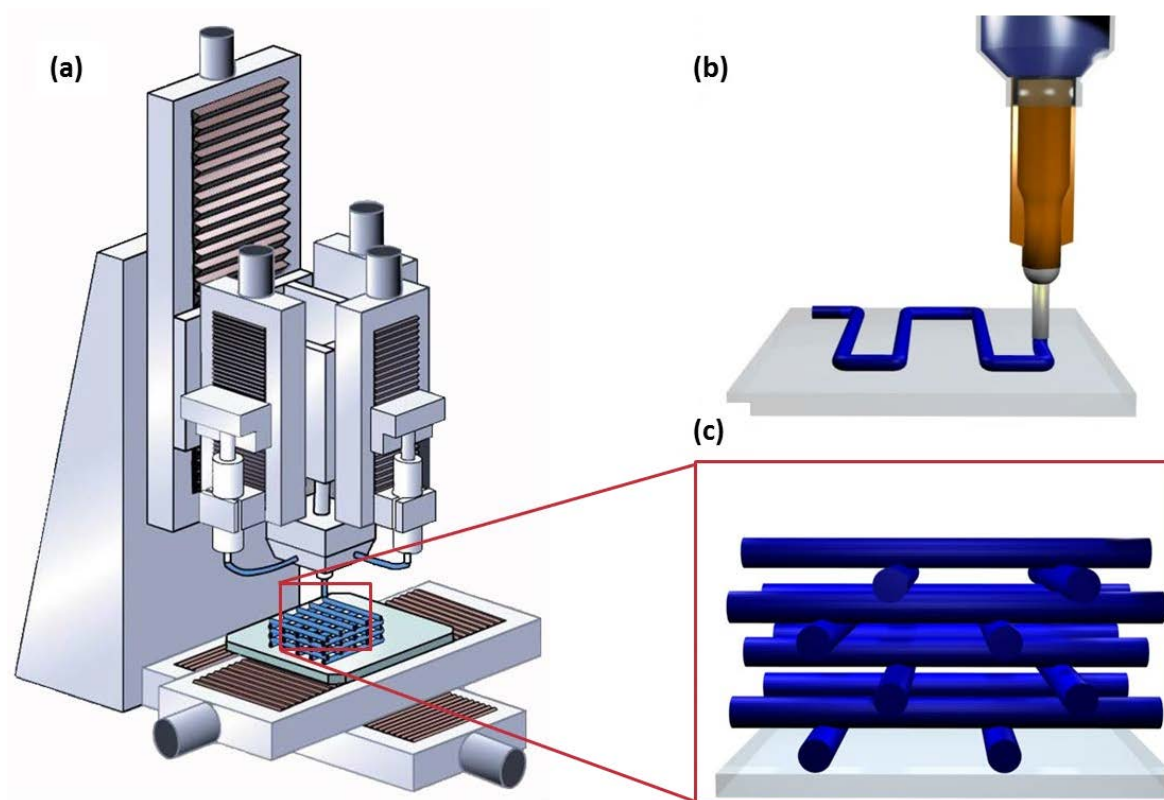


**Figure 3.** Direct-write layer-by-layer fabrication of a 3D periodic structure: schematics of (a) a computer-controlled robot during the deposition,<sup>36</sup> (b) filament deposition in 2D on a substrate, and (c) a close-up view of a periodic microstructure using the direct-write technique.<sup>31</sup>

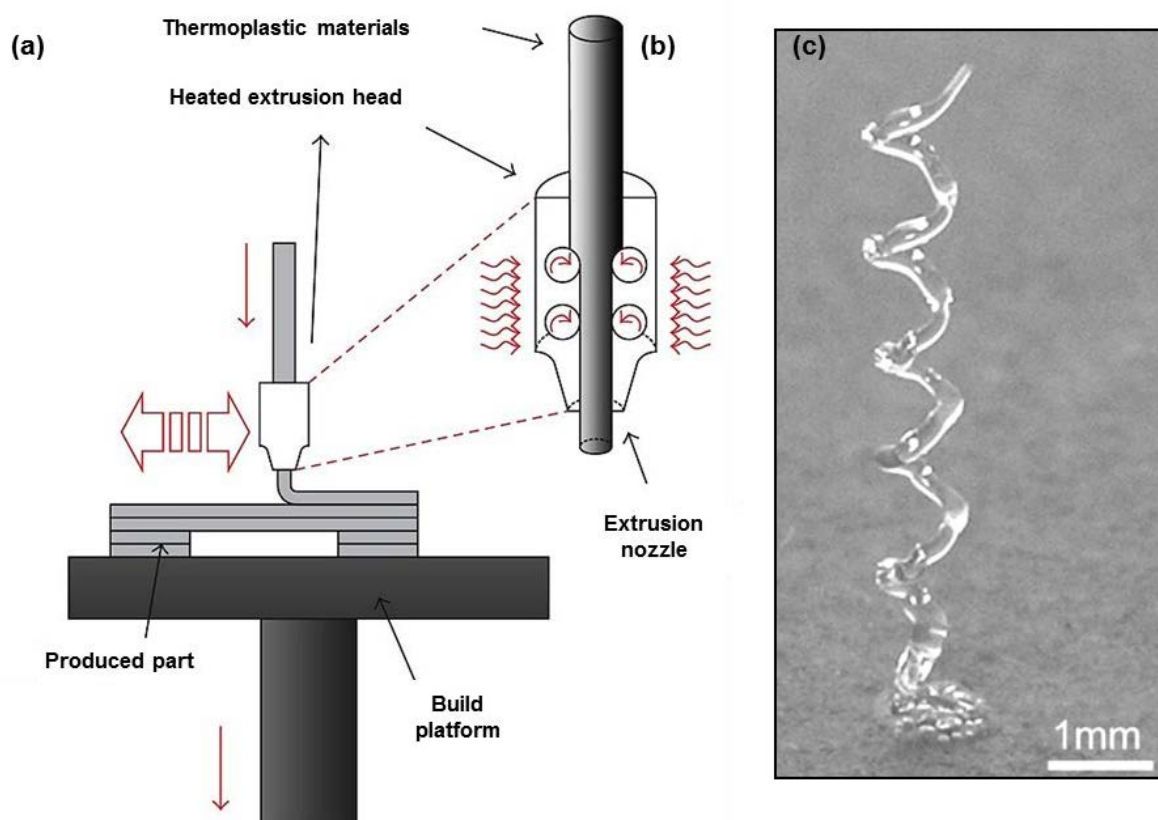


**Figure 4.** FDM fabrication of a helical microstructure made of thermoplastic PLA: (a) schematic representation of the conventional setup composed of heated extrusion chamber, extrusion nozzle and platform (Reproduced from<sup>39</sup>), (b) close-up view of the extrusion nozzle surrounded by the electrical heaters and (c) optical image of a helical microstructure having 5 turns with a pitch of 0.8 mm, filament diameter of 0.2 mm and the coil diameter of 0.9 mm fabricated using thermoplastic PLGA.<sup>21</sup>

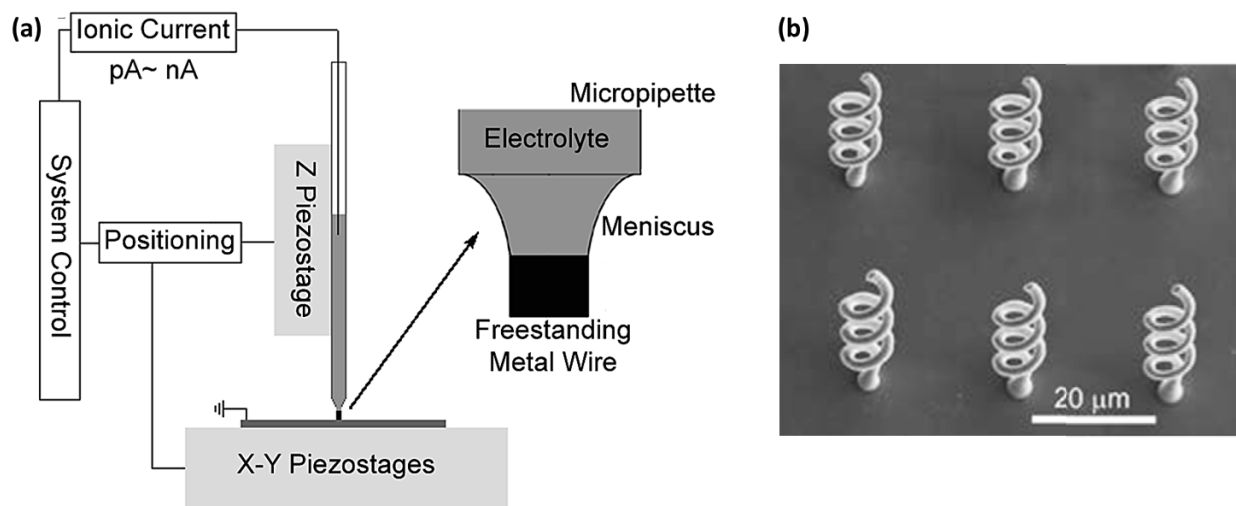


**Figure 5.** MCED fabrication of helical structures: (a) schematic of a basic deposition set-up composed of piezostages and the electrolyte containing micropipette and the dispensing nozzle, and (b) SEM image of six identical microstructures fabricated using copper-based electrolyte solution at room conditions.<sup>48, 49</sup>



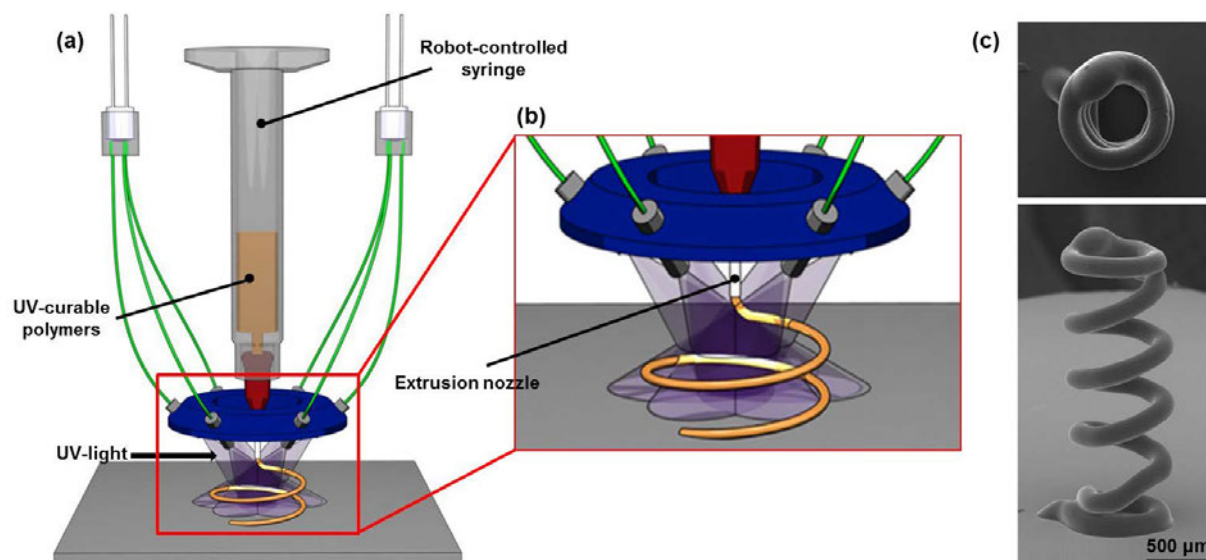


**Figure 6.** UV-3DP fabrication of a photopolymer helical microstructure: (a) schematic representation of the process, (b) close-up view of high intensity UV zone and (c) SEM images of a helical microstructure with circular top-view fabricated at an extrusion speed of 0.3 mm/s and extrusion pressure of  $\sim 2$  MPa using an extrusion nozzle with internal diameter of 150  $\mu\text{m}$  and the urethane-based resin, NEA 123T.<sup>25</sup>

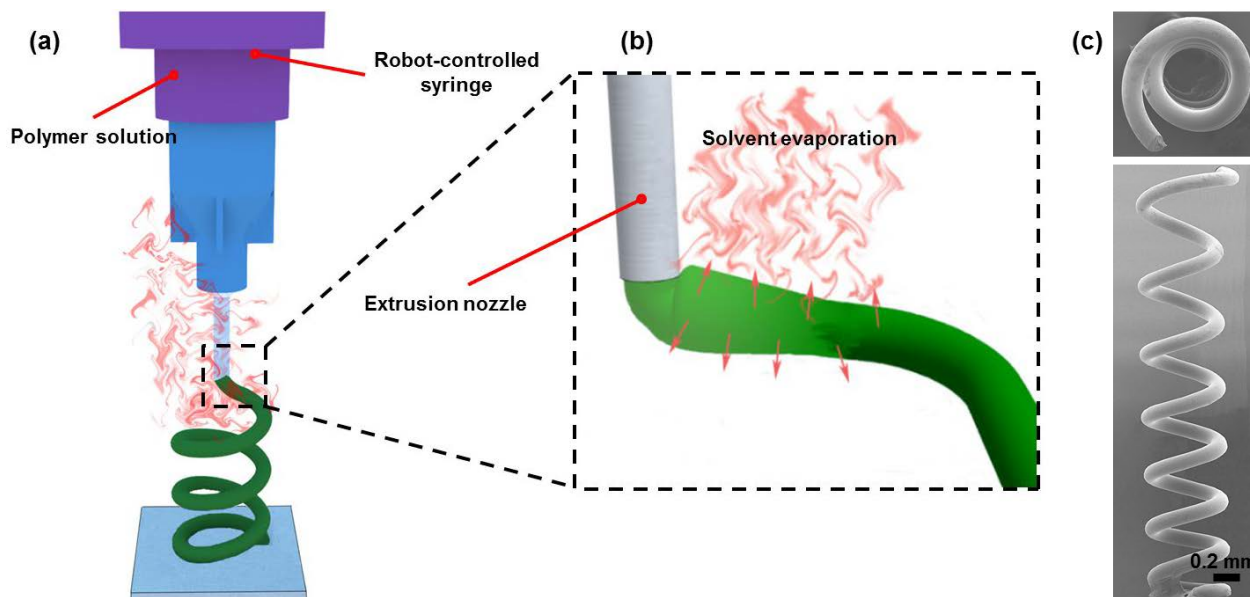


**Figure 7.** SC-3DP fabrication of a helical microstructure made of thermoplastic poly lactic acid (PLA): (a) schematic representation of the process, (b) close-up view of (a) and (c) SEM images of helical microstructure with circular top-view fabricated at an extrusion speed of 0.1 mm/s and extrusion pressure of  $\sim 1.75$  MPa using an extrusion nozzle with an ID of 100  $\mu\text{m}$  and 30 wt.% PLA solution in DCM.<sup>24</sup>

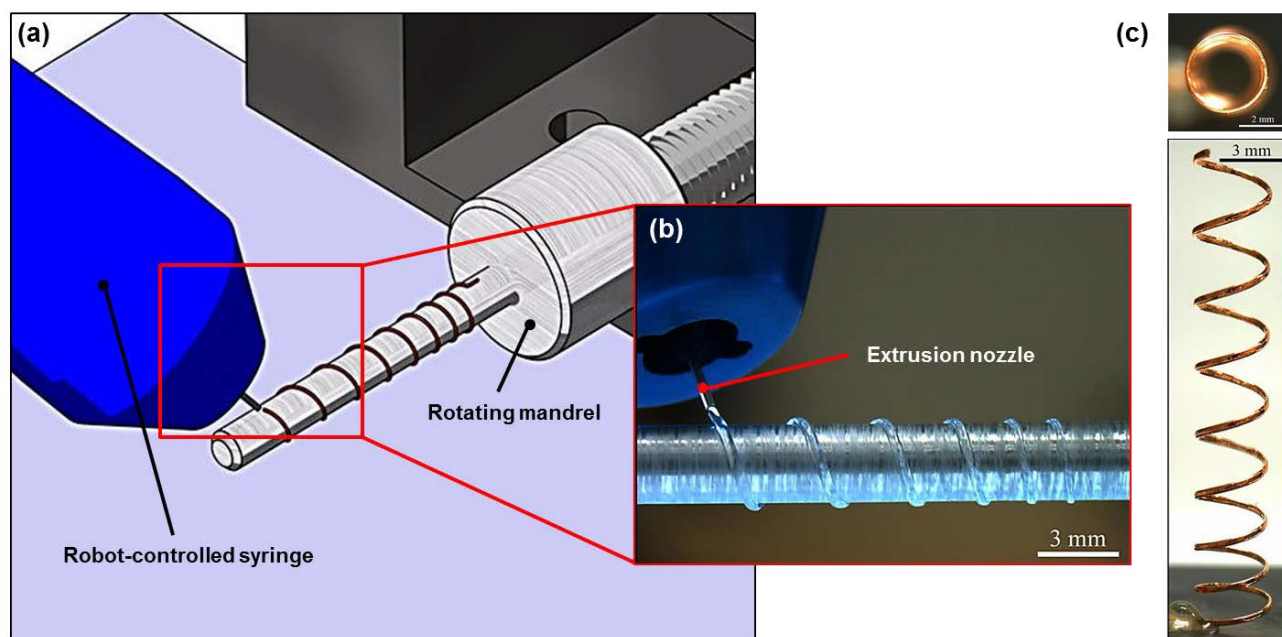


**Figure 8.** CPRM fabrication of a helical microcoil made of thermoplastic poly lactic acid (PLA): (a) schematic representation of the process, (b) an actual close-up optical image of the mandrel, and (c) optical images of copper-coated helical microcoil with circular top-view fabricated using 30 wt.% PLA/DCM solution with an extrusion nozzle of 200  $\mu\text{m}$  internal diameter. The mandrel rotating speed varies while the extrusion pressure is set to  $\sim 2.8$  MPa.<sup>46</sup>

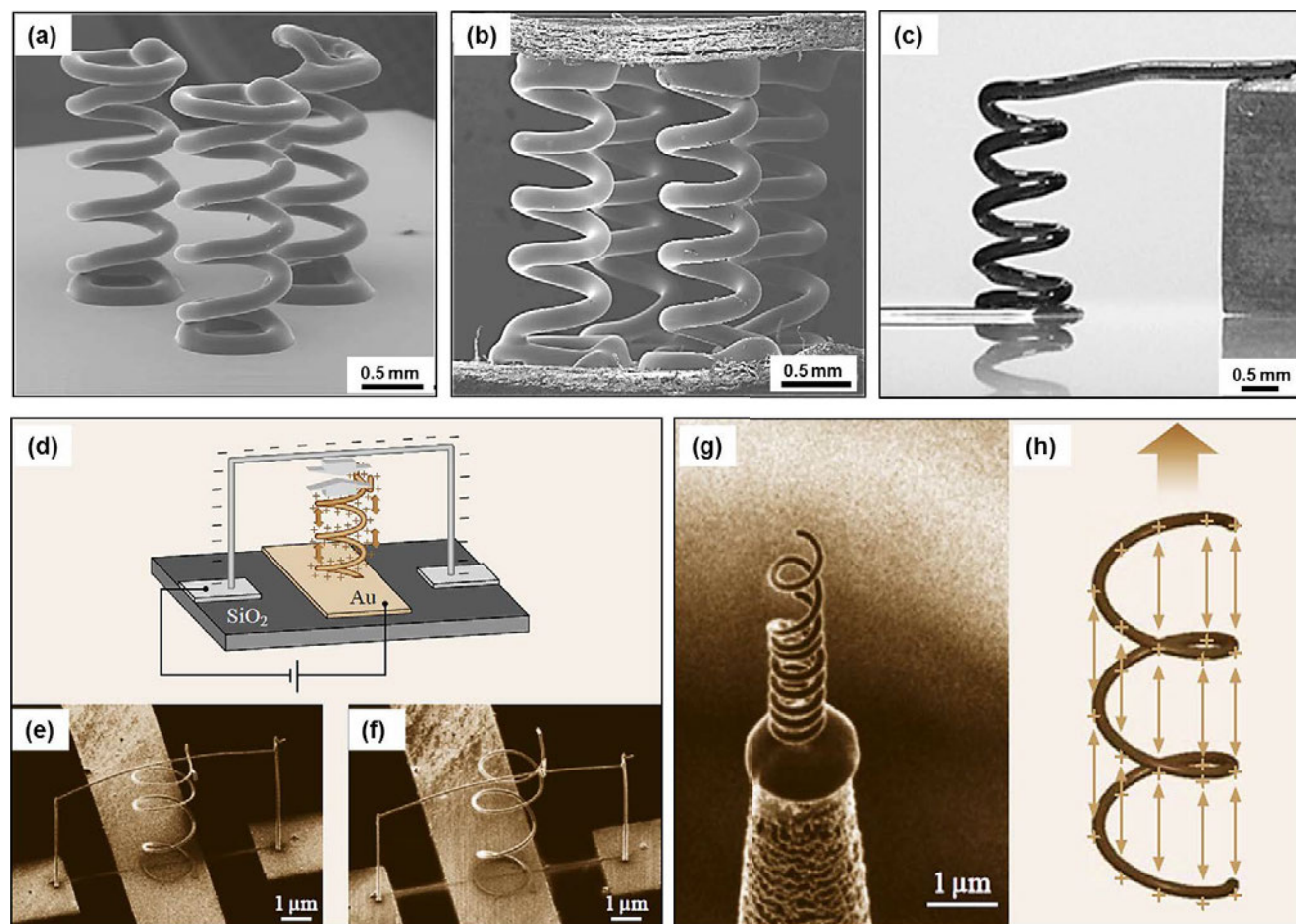


**Figure 9.** (a) SEM image of a triangle array of three helical nanocomposite (urethane-based/0.5 wt.% carbon nanotubes/5 wt.% silica particles) microcoils for potential fluid sensors,<sup>25</sup> (b) SEM image of a 3D nanocomposite (UV-epoxy/1 wt.% carbon nanotubes) sensor capable of sensing out-of-plane displacements,<sup>11</sup> (c) optical image of a nanocomposite (urethane-based/0.5 wt.% carbon nanotubes/5 wt.% silica particles) microcoil connected to two electrodes,<sup>25</sup> (d) schematic of a mechanical switch with its working principle: applying opposite electrical charges to the wiring and the coil results in the formation of repulsive forces between each coil's turn and subsequently the coil extended upward until touching the top wire, (e) and (f) SEM images of the fabricated switch on an Au electrode before and after applying voltage, respectively,<sup>27</sup> (g) SIM image of an electrostatic actuator fabricated on the tip of a Au-coated glass capillary, and (h) schematic illustration of the actuator moving mechanism: the working mechanism of the device is based on the formation of repulsive forces as a result of electric charge accumulation through which leads to the coil expansion.<sup>27</sup>



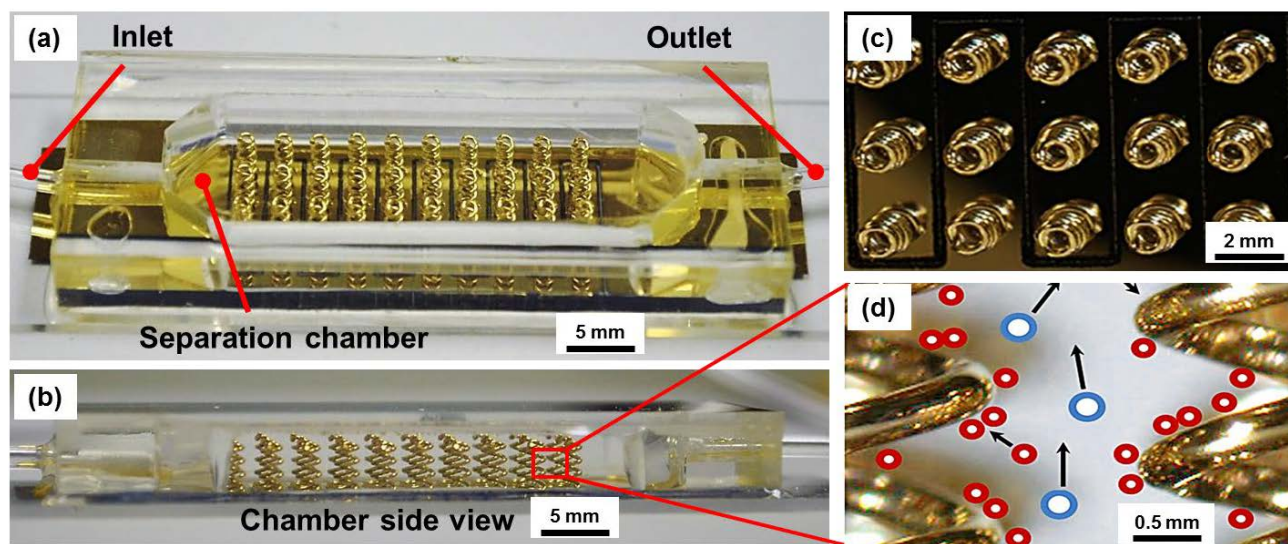


**Figure 10.** Optical images of a microparticle separator using 3D helical-shaped interdigitated microelectrodes: (a) separation chamber composed of 30 gold-sputtered helical microcoils as 3D electrodes, (b) side-view of the chamber, (c) top-view of the 3D electrodes (gold-sputtered microcoils) and (d) representation of the particles (blue and red) separation when passing through two neighboring microcoils.<sup>62</sup>

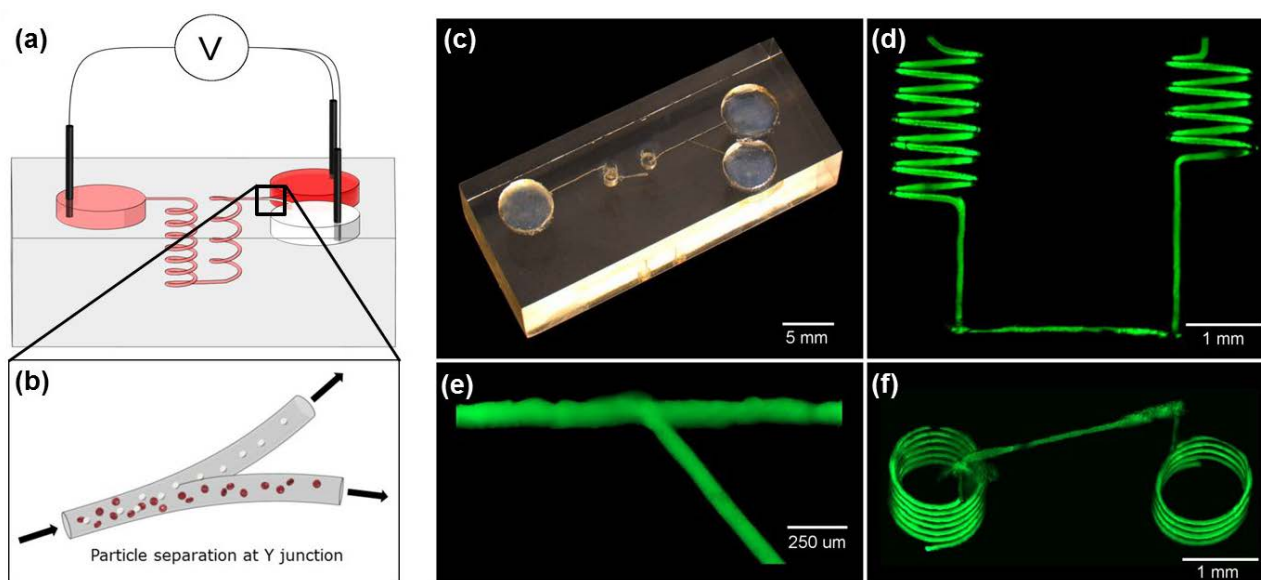


**Figure 11.** (a) Scheme of a 3D particles separator working based on dielectrophoresis forces, (b) schematic representation of particle separation at Y junction, (c) optical image of a real fabricated separator, (d) fluorescent side view image of the helical channels, (e) fluorescent image of the Y junction, and (f) fluorescent slightly inclined bottom view of the separator.<sup>64</sup>

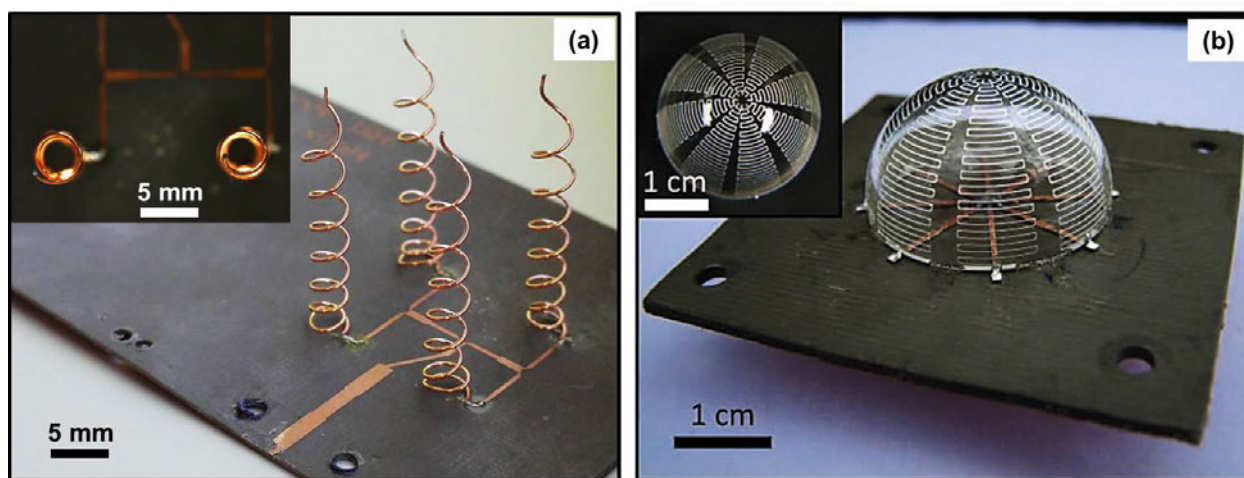


**Figure 12.** (a) optical images of arrays of four micro-antennas using conformal printing method in side and top (inset)<sup>52</sup> and (b) optical images of a micro-antenna fabricated by Adams et al. in side and top (inset).<sup>68</sup>